Articles
doi.org/10.1002/batt.202100116

Chemistry Europe
European Chemical Societies Publishing

Improved Electrochemical Performance of Zinc Anodes by EDTA in Near-Neutral Zinc–Air Batteries

Saul Said Montiel Guerrero,[a, b] Yasin Emre Durmus,*[a] Krzysztof Dzieciol,[a] Shibabrata Basak,[a] Hermann Tempel,[a] Stefan van Waasen,[b, c] Hans Kungl,[a] and Rüdiger-A. Eichel[a, d]

The influence of ethylenediaminetetraacetic acid (EDTA) electrolyte additive on the performance of Zn–air batteries with near-neutral chloride-based electrolytes was examined for primary and secondary batteries. The electrochemical measurements indicated that Zn is not completely active in neat 2 M NaCl, but still could be discharged up to 1 mA cm^{-2} around −1.0 $V_{Ag/AgCl}$. The characterization of the Zn surfaces revealed the existence of a passive film consisting of Simonkolleite, $Zn(OH)_2$, and/or ZnO. The EDTA additive enhanced the discharge voltages by 200 mV to −1.2 $V_{Ag/AgCl}$ indicating an active Zn surface. The effect of EDTA is explained by its chelation abilities with Zn^{2+} before formation of hydroxide or oxide species. The Zn–air cells with EDTA were operated up to 930 h with specific energies up to 840 Wh kg_{Zn}^{-1}. The cells could also be cycled up to 70 cycles while providing enhanced discharge voltages at 1.15 V over 50 cycles. The positive effect of EDTA is dependent on the amount of free EDTA molecules. Nevertheless, the Zn–air cells showed better performance in terms of higher discharge voltage, discharge energies, and lower overpotentials in presence of EDTA.

1. Introduction

In recent years, metal–air batteries have attracted much attention as one important line of development towards resource efficient, environmentally friendly, and high energy density electrochemical storage systems.[1–5] Among various possible chemistries, zinc-based metal–air batteries are the most advanced for both primary and secondary applications. Primary aqueous Zn–air batteries have already been available since the 1930s and nowadays successful advancements can commercially be found in low-power telecommunication and medical applications. Secondary Zn–air batteries, however, are still facing challenges especially in alkaline electrolytes which hinder their advances towards further development and commercialization.[6,7]

Theoretically, Zn–air batteries have the potential to provide specific energies of 1352 Wh kg_{Zn}^{-1} and energy densities of 9653 Wh L_{Zn}^{-1}. From the practical performance point of view, primary Zn–air batteries can provide specific energies of 500–700 Wh kg_{Zn}^{-1} when related to anode mass only.[8,9] A comparison to Li-ion batteries at a coin cell level also shows prominent results for Zn–air batteries in terms of specific energies and volumetric energy densities; 500 Wh $kg_{Zn\,cell}^{-1}$ and 1400 Wh $L_{Zn\,cell}^{-1}$ vs. 350 Wh $kg_{Li\,cell}^{-1}$ and 810 Wh $L_{Li\,cell}^{-1}$.[10,11] Secondary Zn–air batteries, however, suffer from several challenges and thus, depending on the depth of discharge, can only provide specific energies up to 500 Wh kg_{Zn}^{-1} with a cycle life typically limited to several hundreds of cycles.[9–13] The main challenges for limited performance can be attributed to the nature of alkaline electrolyte in which air cathodes and Zn anodes face issues such as inefficient electrocatalysts, unstable carbon-based air electrode, CO_2 uptake from ambient air, dendrite formation, corrosion and limited cyclability of Zn anodes. Although Zn anode related obstacles may be reduced to an extent by using corrosion inhibition additives or excess amount of Zn etc., the obstacles remaining at the air cathode also hinders the performance. The insoluble carbonate formation upon CO_2 uptake from the ambient air results in electrolyte consumption and pore clogging at the air cathode. Moreover, sluggish kinetics toward O_2 reduction and evolution reactions and degradation of the bifunctional catalysts are other major factors that impede the efficient use of rechargeable Zn–air batteries. Nevertheless, the alkaline Zn–air batteries remain as the most advanced systems and can provide highest specific energies.[11]

[a] S. S. Montiel Guerrero, Dr. Y. E. Durmus, Dr. K. Dzieciol, Dr. S. Basak, Dr. H. Tempel, Dr. H. Kungl, Prof. Dr. R.-A. Eichel
Fundamental Electrochemistry (IEK-9)
Forschungszentrum Jülich GmbH
Jülich, Germany
E-mail: y.durmus@fz-juelich.de
[b] S. S. Montiel Guerrero, Prof. Dr. S. van Waasen
Department of Electrical Engineering and Information Technology
University of Duisburg-Essen
Duisburg, Germany
[c] Prof. Dr. S. van Waasen
Central Institute of Engineering, Electronics and Analytics – Electronic Systems (ZEA-2)
Forschungszentrum Jülich GmbH
Jülich, Germany
[d] Prof. Dr. R.-A. Eichel
Institute of Physical Chemistry
RWTH Aachen University
Aachen, Germany

Supporting information for this article is available on the WWW under https://doi.org/10.1002/batt.202100116

Currently, there are several strategies focusing their effort to overcome some of the aforementioned challenges by developing alternative aqueous,[14–19] non-aqueous,[1] even solid-state[20,21] Zn–air batteries. Among these, for example, the neutral or near-neutral electrolytes can provide solutions to corrosion of Zn anode, dendrite formation, and carbonization of the electrolyte. Mostly ammonium chloride (NH_4Cl) is used as the standard salt for such electrolytes. Although the history of NH_4Cl-based batteries (zinc-carbon or Leclanché batteries) dates back to the 19th century,[22,23] the first concept to utilize it in the primary Zn–air battery was published by Jindra et al. in 1973[24] and in the secondary Zn–air battery by Amendola et al. in 2012.[25]

In following years, the development of NH_4Cl-based Zn–air batteries was focused on the optimization of the electrolyte content to improve the battery performance. In 2014 and 2016, Goh et al.[26] and Sumboja et al.[14] developed a secondary Zn–air battery with an electrolyte consisting of NH_4Cl + Zinc chloride ($ZnCl_2$) with additives (polyethylene glycol or thiourea) which were used to improve the deposition of the Zn ions more homogeneously during cycling. Utilizing such electrolytes in the secondary Zn–air batteries resulted in extended operation times up to 5,100 h with 540 cycles (at low depth of discharge); nonetheless, it was suggested that the performance could be further improved by better performing electrocatalysts and tuning the electrolyte properties.[14] In 2017, Clark et al. presented the first continuum model of $NH_4Cl + ZnCl_2$ based secondary Zn–air batteries to optimize the electrolyte composition and the cell design while considering the pH stability and final discharge products.[27] The model was further developed and validated by experimental methods such as galvanostatic cycling, operando pH experiments, XRD, and EDX characterization of the surfaces.[28] Accordingly, the performance of the Zn–air battery could be well evaluated and the potential obstacles were highlighted. In a recent study, Durmus et al. performed electrochemical investigations on the applicability of Zn–Al alloys and Zn electrodes in neutral Zn–air batteries with NaCl electrolyte.[29] In comparison to Zn electrodes, the influence of Al alloying was reported as temporarily enhanced discharge potentials in 2 M NaCl electrolytes with pH 7.

In general, the field of electrolyte additives for aqueous Zn–air batteries is quite extensive due to the different desired effects. While some of the additives[30–32] are used to enhance the charge efficiencies by shifting the hydrogen evolution potential to higher values in order to further improve the metal deposition, other electrolyte additives are also used for prevention of the dendrite formation[32] and homogeneous deposition,[33] reduction of the corrosion reaction[34,35] or chelation and pH stabilization.[16] Concerning the EDTA additive, previous plating studies of sodium nitrate,[36] alkaline,[37] choline chloride,[38,39] and acidic sodium chloride-based[40] solutions containing Zn-EDTA chelates showed the possibility of Zn electrodeposition from the dissolved Zn-EDTA complexes. However, the overall performance of a Zn–air batteries with near-neutral electrolytes containing EDTA is still an open question.

The present work, therefore, evaluates the influence of Ethylenediaminetetraacetic acid (EDTA) additive on the performance of near-neutral secondary Zn–air batteries. The chelating properties of EDTA are widely known and used in several fields as complexing agent for metal ions.[41,42] Basing on these properties, the electrochemical behavior of Zn electrodes were investigated in 2 M NaCl solutions with pH 10 in the presence and absence of EDTA additive. The corrosion parameters of the Zn electrodes were extracted from potentiodynamic polarization experiments. The intermediate term (24 h) discharge experiments were performed under current densities of 0.1, 0.25, 0.5, and 1 $mA\,cm^{-2}$ in a three-electrode setup. Subsequent to the discharge, the surface of the electrodes were further characterized by laser scanning microscope (LSM), X-ray diffraction (XRD), and scanning electron microscope (SEM) in order to analyze the dissolution behavior and the discharge products. The performance of full-cell Zn–air batteries were evaluated in galvanostatic discharge experiments (in primary-mode) up to 930 h and in galvanostatic cycling experiments (in secondary-mode) up to 575 h with 70 cycles. In comparison to neat electrolyte, the influence of EDTA additive was shown to enhance specific energies and mass utilization efficiencies.

2. Results and Discussion

2.1. Open Circuit Potential and Potentiodynamic Polarization

Figure 1a shows the OCP profiles of Zn in 2 M NaCl at pH 10, in absence (black curve) and presence (red curve) of EDTA. The potential of Zn in neat 2 M NaCl starts at initial values of around −1.05 $V_{Ag/AgCl}$, slightly increasing to −1.11 $V_{Ag/AgCl}$ after 2 h and then slowly decays to −1.06 $V_{Ag/AgCl}$ after 24 h, while the potential of Zn in 2 M NaCl with 0.1 M EDTA is stable at around −1.22 $V_{Ag/AgCl}$ during the 24 h of OCP experiment. Thus the addition of EDTA to the 2 M NaCl results in an increase of the potential of about 170 mV.

The increase of the initial potential towards more negative values along the first 2 h of the Zn in the 2 M NaCl could be attributed to the slow adsorption of OH^- ions present in the electrolyte. Subsequently, slight decay of the potential is resulted from the drop on the pH value due to the lack of buffering capabilities of NaCl solutions.[41,43] According to the Pourbaix diagram of Zn (Figure 1b), the cell potential slightly decreases (around 160 mV) when the pH changes between 11 and 8.5.[44,45] Measurement of the pH of the electrolyte after the 24 h of OCP supports this observation, since the pH drops from pH 10 to values around pH 8 while there is also 50 mV decrease on the electrode potential. The limited decay of the electrode potential can be due to the quasi-passive state of the Zn surface since it is not completely active. In line with the Pourbaix diagram,[44,45] the potential of Zn at pH 10 should be around −1.25 $V_{Ag/AgCl}$ (−1.03 V_{SHE}). However, the experimental results indicate that the surface of Zn is in a quasi-passive state since the potential of the Zn in the neat 2 M NaCl is lower than the expected value. On the other hand, addition of EDTA to the

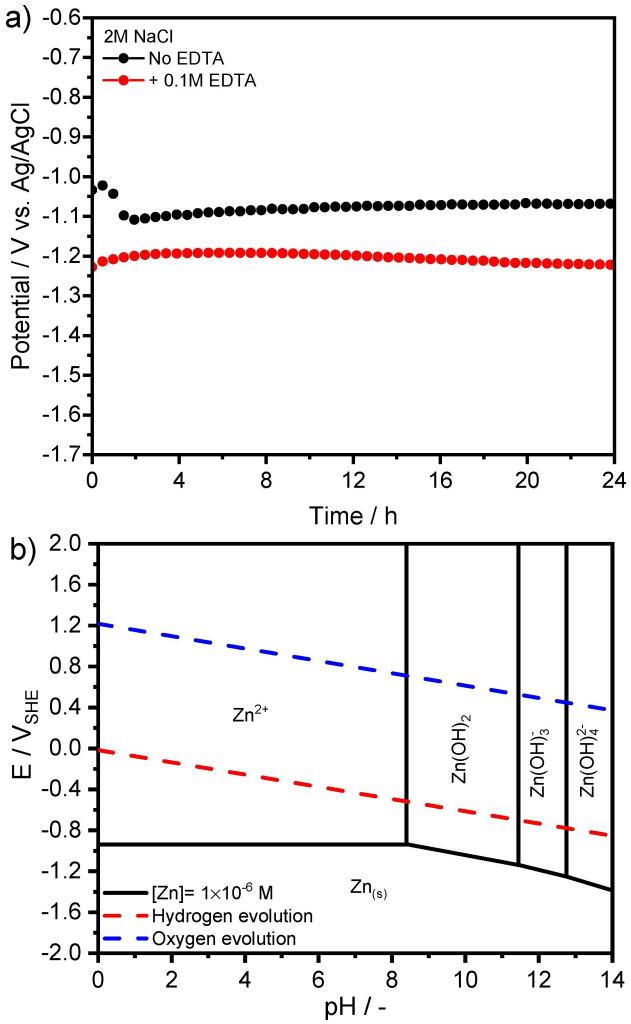

Figure 1. a) OCP profiles of Zn in 2 M NaCl at pH 10 in absence (black curve) and presence of 0.1 M EDTA (red curve). b) Pourbaix diagram of Zn adapted from Beverskog et al.[45] The diagram shows the stability range of the stable uncharged aqueous complex $Zn(OH)_2$ before passivation (in form of ZnO) at Zn concentrations $\geq 10^{-5.7}$.

2 M NaCl results in an enhanced potential to −1.22 $V_{Ag/AgCl}$, which is similar to the potential given by the Pourbaix diagram.

The enhancement of the potential in presence of EDTA can be attributed to two main factors: (1) the chelating properties of EDTA, and (2) an increase of the pH stability of the NaCl electrolyte. The chelation process (or complexation) prevents the formation of insoluble species of Zn, resulting in highly soluble Zn-EDTA complexes. However, EDTA can be present as several dissociated species (6 possible deprotonated species) depending on the pH, where the completely deprotonated species are more effective for complexation (30% EDTA is fully dissociated at pH 10[41]). The addition of EDTA to the 2 M NaCl solution increases the pH stability of the electrolyte, as observed from the almost unaffected pH of the electrolyte after the 24 h of OCP experiments in presence of EDTA. Also, the higher potentials with EDTA in comparison to neat NaCl solution corroborates the absence of a passive film on the Zn surface.

Possible mechanisms of the interaction between the Zn and EDTA can be found in the literature, among which Ryczkowski[46] demonstrated via (PA) FT-IR (Photoacoustic Fourier transform infrared spectroscopy) that EDTA could be adsorbed on some inorganic oxides and hydroxides. Different adsorption mechanisms were proposed depending on the pH of the solution and the nature of the metal surface involved in the chelation, namely if it consisted of oxides, hydrous oxides, hydroxides, oxyhydroxides, hydrous or superficially hydrated oxides.[46,47] Moreover, previous studies have shown that EDTA is capable of leaching metal ions from oxides or hydroxides.[48–50] Hence, similar mechanisms could also be the origin of the EDTA influence on the Zn potentials shown in this study.

Further experiments were performed by potentiodynamic polarization method to get more insights on the possible influence of EDTA on the electrochemical behavior of Zn in NaCl electrolytes. Figure 2 shows the potentiodynamic polarization of Zn in neat 2 M NaCl (black curve) and in presence of 0.1 M EDTA (red curve). The corrosion parameters were obtained by Tafel fit in the range of ±50 mV of the corrosion potential (E_{corr}) and are summarized in Table 1.

The E_{corr} of Zn in neat 2 M NaCl is around −1.25 $V_{Ag/AgCl}$, while addition of EDTA shifted the E_{corr} to −1.32 $V_{Ag/AgCl}$. The corrosion current densities are obtained as 4.75 and 5.39 μA cm^{-2} in absence and presence of EDTA, respectively. Both curves show a shoulder at around −1.08 V without EDTA and −1.0 V in presence of EDTA. These shoulders resemble a

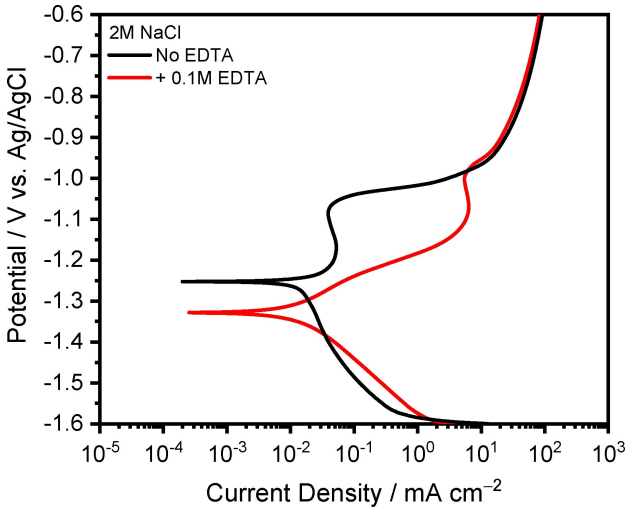

Figure 2. Potentiodynamic polarization of Zn in 2 M NaCl at pH 10 in absence (black curve) and presence of 0.1 M EDTA (red curve).

Table 1. OCP values and corrosion parameters derived from potentiodynamic polarization of Zn in 2 M NaCl at pH 10.

EDTA	OCP after 24 h [mV]	Potentiodynamic polarization E_{corr} [mV]	J_{corr} [μA cm^{-2}]
–	−1070	−1255.5 ± 4.7	4.8 ± 0.9
0.1 M	−1220	−1323.0 ± 6.9	5.4 ± 0.8

passivation peak, where the current slightly decreases as the anodic scan continues. However, the current densities continue increasing at potentials more anodic than the semi-passivation peak, indicating that the Zn could still readily react. The rapid increase on the current densities originate from pitting caused by the chloride ions, which starts at around $-1.05\ V_{Ag/AgCl}$ ($E_{pitting}$).[22]

The slight decrease on the current densities between E_{corr} ($-1.25\ V_{Ag/AgCl}$) and $E_{pitting}$ ($-1.05\ V_{Ag/AgCl}$) during the potentiodynamic polarization of Zn in neat 2 M NaCl confirms the existence of a passive film. On the contrary, the potentiodynamic polarization of the Zn in presence of 0.1 M EDTA shows less significant passivation peak, but a higher E_{corr} and larger current densities in the range from E_{corr} ($-1.32\ V_{Ag/AgCl}$) to $E_{pitting}$ $-1.05\ V_{Ag/AgCl}$) in comparison to the solutions not containing EDTA. Under high anodic polarizations ($>-1.0\ V_{Ag/AgCl}$), the current response of the Zn for both solutions shows almost identical behavior; hence, it suggests that there might be a limiting current for the effectivity of EDTA on the enhanced potentials but no visible adverse effect in comparison to neat electrolyte.

The fact that the OCP is more positive than the E_{corr} for the solutions with and without EDTA can be explained through the cathodic corrosion of Zn in chloride solution.[51] As proposed by Baugh,[52] water reduction occurs at potentials more cathodic than $-1.37\ V_{Ag/AgCl}$ on Zn in chloride based solutions according to the following reaction [Eq. (1)]:

$$2H_2O + 2e^- \rightarrow 2OH^- + H_2 \quad (1)$$

Since the present polarization experiments start at $-1.6\ V_{Ag/AgCl}$, OH^- ions from hydrolysis could be produced in relatively high amounts. Upon the local concentration increase of the produced OH^- ions, "local alkalization" can occur on Zn resulting in cathodic corrosion.[51,53] Although the Zn is immersed in near-neutral electrolyte, local dissolution of a possible passive layer could also be expected similarly as in the alkaline electrolytes.[22] Furthermore, Prestat et al. studied the reaction products of Zn under prolonged cathodic potentials in near-neutral NaCl media, where Raman microscopy and X-ray diffraction revealed the presence of metallic Zn after holding a cathodic potential of $-1.27\ V_{Ag/AgCl}$ for at least 17 h. It was reported that ZnO is mainly present in the range from -1.04 to $-1.26\ V_{Ag/AgCl}$, while Simonkolleite mainly appears at potentials anodic to $-1.01\ V_{Ag/AgCl}$.[51] Thus, the reaction products on Zn electrodes show differences depending on the potentials that were applied and most likely, also on the polarization durations.

According to the potentiodynamic polarization curves, the observed E_{corr} of Zn in 2 M NaCl without EDTA (Figure 2) corresponds to the potential of neat Zn, which is activated by the cathodic polarization. Further evidence for the cathodic activation of Zn can be found in the previous studies which report the polarization curves of Zn electrodes in NaCl solutions.[53–55] If the initial scan potential for the potentiodynamic polarization is more cathodic than the water reduction potential ($<-1.37\ V_{Ag/AgCl}$), the resulting E_{corr} is also more negative than the commonly reported open circuit potentials ($<-1.05\ V_{Ag/AgCl}$), which is in good agreement with the present work. Contrariwise, the corrosion potential of Zn near $-1.05\ V_{Ag/AgCl}$ is usually obtained when the initial scans start at more positive values than the water reduction potential.[56,57] Therefore, it can be stated that neither the NaCl concentration, pH, scan rate, electrode area, immersion time nor counter electrode have no influence on the resulting E_{corr} derived from the potentiodynamic polarization. On the other hand, the reported E_{corr} is more dependent on the potential at which the potentiodynamic experiments were started.

In contrast to the neat 2 M NaCl electrolyte, the resulting polarization curve of the electrolyte containing 0.1 M EDTA is affected by the cathodic activation, only at a minor degree. More specifically, the difference between the OCP and E_{corr} in the electrolyte without EDTA is around 185 mV, while for the electrolyte containing 0.1 M EDTA is around 102 mV. In the OCP profiles, however, the overall enhancement of the potential with the addition of EDTA to the electrolyte is around 150 mV, and the increased potential is stable without the necessity of a cathodic polarization. This effect can be attributed to the chelation properties of EDTA and the increased pH stability of the NaCl solutions containing 0.1 M EDTA due to its buffering capabilities.

2.2. Galvanostatic Discharge/Half-Cell Stripping

As previously examined by the OCP profiles and potentiodynamic polarization experiments, the Zn is in a quasl-passivated state in the 2 M NaCl, while addition of EDTA allegedly hinders the formation of a passive film resulting in a more active metallic Zn surface. The semi-passivated (without EDTA) and activated (with EDTA) state of Zn was further investigated under several anodic current densities (galvanostatic discharge or half-cell stripping) as presented in Figure 3.

Figure 3a shows a stable discharge potential of Zn in neat 2 M NaCl at around $-1.03\ V_{Ag/AgCl}$ under 0.1 to 1 mA cm^{-2} anodic currents, while the discharge potential of Zn in EDTA containing electrolyte (Figure 3b) is around $-1.25\ V_{Ag/AgCl}$ under 0.1 and 0.25 mA cm^{-2}. The resulting potential of Zn in presence of EDTA is initially lower at $-1.14\ V_{Ag/AgCl}$ under 0.5 mA cm^{-2} and at $-1.1\ V_{Ag/AgCl}$ under 1 mA cm^{-2}, but in both cases the

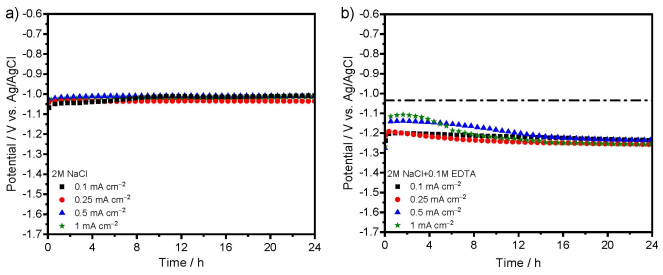

Figure 3. Galvanostatic half-cell discharge of Zn in 2 M NaCl at pH 10 under 0.1, 0.25, 0.5 and 1 mA cm^{-2} in a) absence of EDTA and in b) presence of 0.1 M EDTA. The abscissa in (b) illustrates the average discharge potential of the Zn electrodes in the neat electrolyte (obtained from (a)).

potential increases to $-1.25\ V_{Ag/AgCl}$ within 12 hours. The reason for this gradual shift to more negative discharge potentials upon 0.5 and 1 mA cm^{-2} in presence of EDTA is still unknown and needs further investigation. Overall, the average discharge potentials are 220 mV more negative for all the applied currents on Zn in presence of 0.1 M EDTA and directly increase the power output in comparison to the Zn discharged in neat 2 M NaCl.

According to Pourbaix diagram,[44,45] the immunity region of metallic Zn remains below the stability window of water in aqueous solutions and therefore Zn dissolves while producing H_2. Zn is in the "passive" regime at pH 10 and should not display potentials at around $-1.25\ V_{Ag/AgCl}$. The discharge potential of Zn in the neat electrolyte at pH 10 is not significantly different in comparison to discharge behavior in 2 M NaCl with pH 7.[29] The lack of enhanced potential at pH 10 could be partially explained by the poor pH stability of neat NaCl solutions, since the pH of such solutions is dependent on the salt concentration and the resulting effect on the activities of H^+ and OH^-.[41] Experimentally, the poor pH stability of neat NaCl is confirmed by the pH drop from 10 to around 8 after the galvanostatic discharge (pH of the solutions were measured before and after the experiments by the pH electrode). Thus, lower pH values also contribute to lower potentials of Zn in accordance with Pourbaix. The almost unaffected discharge potential under different current densities (Figure 3a) in the neat electrolyte suggests the discharge of Zn continues through pitting mechanism, which agrees with the results from the potentiodynamic polarization experiments. Moreover, the possible presence of a passive film seems to reduce the potential of Zn, but does not inhibit the dissolution.

In order to understand the possible origin of such passive film in presence of neat NaCl, reaction mechanisms of Zn during discharge is hereby provided. As previously discussed, Zn spontaneously reacts in aqueous solutions as follows [Eq. (2)]:

$$Zn_{(s)} \rightarrow Zn^{2+}_{(aq)} + 2e^- \quad (2)$$

According to McMahon et. al.,[43] the Zn^{2+} ion is quite abundant at low Cl^- concentrations (0.06 M), while its ion fraction is almost zero at high Cl^- concentrations (5.45 M). Accordingly, Zn^{2+} is not stable in 2 M NaCl and will tend to further react as follows [Eqs. (3), (4)]:

$$Zn^{2+}_{(aq)} + 2OH^- \rightarrow Zn(OH)_2 \quad (3)$$

$$5Zn^{2+} + 8OH^- + 2Cl^- + H_2O \rightarrow Zn_5(OH)_8Cl_2 \cdot H_2O \quad (4)$$

For simplicity, the $Zn_5(OH)_8Cl_2 \cdot H_2O$ reaction product will be referred hereafter as Simonkolleite, which is a white and low water soluble powder. Upon saturation, the continuously produced $Zn(OH)_2$ from Equation (3) can further react depending on the local pH and Cl^- concentration as follows [Eqs (5)–(7)]:

$$Zn(OH)_2 \rightarrow ZnO + H_2O \quad (5)$$

$$Zn(OH)_2 + 2OH^- \rightarrow Zn(OH)_4^{2-} \quad (6)$$

$$5Zn(OH)_2 + 2Cl^- + H_2O \rightarrow Zn_5(OH)_8Cl_2 \cdot H_2O + 2OH^- \quad (7)$$

The formation of ZnO requires a dehydration of a stable layer of $Zn(OH)_2$ upon local saturation, as described by Equation (5). Under anodic conditions, the production of $Zn(OH)_2$ increases and the saturation is faster reached, which possibly promotes the production of ZnO. Given the bulk conditions of the neat 2 M NaCl, production of zincates ($Zn(OH)_4^{2-}$) can occur only at a minor degree in near-neutral electrolytes since it requires high pH conditions. Prestat et. al. could mainly identify Simonkolleite at potentials close to $-1.02\ V_{Ag/AgCl}$ while ZnO is mainly found at $-1.12\ V_{Ag/AgCl}$ in 0.6 M NaCl solutions.[51] In accordance with the potentials observed in the discharge experiments ($-1.03\ V_{Ag/AgCl}$), a mixture of reaction products Simonkolleite, ZnO and $Zn(OH)_2$ could be expected, where a thin but still present layer $Zn(OH)_2$ is the intermediate compound before the formation of ZnO and Simonkolleite.[51,52] These products are the compounds of the passive film.

Furthermore, depending on the applied currents, white flake-like precipitates were present in the electrolyte at the end of the experiments. For instance, after 24 h discharge at 1 mA cm^{-2} there is an appreciable amount of precipitates, while the electrolyte is relatively clear after 24 h at 0.1 mA cm^{-2}. Table S1 (Supporting Information) shows a summary of the physical properties of the possible reaction products of Zn in NaCl electrolytes. $Zn(OH)_2$, ZnO and Simonkolleite are all white precipitates and are between 127 and 234% larger in volume than the metallic Zn. The volume increase of the reaction products and the subsequent mechanical stress produced could partially explain the presence of such precipitates.

A possible way to decrease or even completely prevent the formation of a passive film on the Zn surface could be achieved by using complexing agents in the electrolyte, which are widely used in chemistry due to their chelation properties with metallic ions. The resulting complex species are highly soluble in water.[41] In the chelation process, the metallic ion is surrounded by the complexing agent and the reaction between the metallic ion and the surrounding media is reduced. The bonding strength between the metallic ion and the complexing agent is indicated by the magnitude of the chelation stability constants, where higher values result in more stable complexes. The increase on the discharge potential of Zn upon addition of EDTA to the 2 M NaCl could be therefore attributed to the relatively high chelation stability constant of EDTA with the Zn^{2+} ions (16.5) and the continuous solvation of the resulting Zn-EDTA complex in the electrolyte.[41] Thus, the formation of passive species adsorbed on the Zn surface is most likely hindered.

With respect to the pH stability of the NaCl solutions, formation of zinc hydroxide or Simonkolleite according to the Equations (3) and (4) lead to consumption of hydroxyl ions; thus pH tends to decrease as confirmed by the discharge

experiments. Contrariwise, the presence of EDTA in the solutions stabilizes the pH of NaCl solutions during the discharge, as confirmed by the pH still close to 10 after the 24 h discharge experiments, due to complexing Zn^{2+} ions before the other possible reactions that would consume OH^- ions can take place. Furthermore, in accordance with previous studies,[48–50] EDTA can be adsorbed on the surface of ZnO or even leach the ions from the respective oxide or hydroxide, which adds up to the synergetic effects of addition of EDTA to the 2 M NaCl on discharge performance.

2.3. Characterization of the Zn Surfaces

Laser scanning microscopy (LSM) investigations have been performed to gain better insights into the surface morphologies of the Zn after galvanostatic discharge experiments. Figure 4 shows the 3D LSM images of the Zn samples after 1 and 24 h discharge with 1 mA cm^{-2} in presence and absence of EDTA. The surface of Zn after 1 h of discharge for both electrolytes show a similar roughness of less than 10 µm, as shown in Figures 4a and c. However, Zn shows a thin film with some areas exposing a metallic surface underneath after discharge in neat 2 M NaCl (see Figure S1) while the Zn discharged in presence of EDTA shows a more homogeneous surface and no film or other particulates on the surface.

More remarkable differences appear after 24 h of discharge, where the surface of the Zn in neat 2 M NaCl has height differences up to 100 µm, as seen in Figure 4b. Within the large pits, a metallic Zn surface was visible (blue regions), suggesting that some areas of the metallic anode were continuously exposed during the 24 h of discharge upon partial breakage of the passive film (yellow and orange regions). Conversely, the Zn discharged in the solutions containing 0.1 M EDTA shows a surface roughness of around 40 µm (Figure 4d) and no apparent layer or particulates were observed. Thus, these findings confirm that the presence of EDTA effectively suppresses the formation of a passive film. The absence of any solids on the Zn surface after discharge also indicates that all the discharged product of Zn is dissolved in the electrolyte.

In addition to the characterization of the surface morphologies by LSM, the chemical nature of the surfaces of the Zn electrodes after discharge was analyzed by X-ray diffraction (XRD). Figure 5 shows the XRD patterns of the Zn samples that were discharged under 1 mA cm^{-2} for 24 h in 2 M NaCl with and without EDTA.

In Figure 5a, both patterns (purple and yellow) show that the Zn surface is mostly in metallic state while the Zn surface discharged in neat electrolyte also reveals some extra peaks which indicate the presence of Simonkolleite (Figures 5b and c). However, on both electrodes neither ZnO nor $Zn(OH)_2$ could be detected, as shown in the enlarged area in Figure 5c. Furthermore, the white precipitates in the neat 2 M NaCl electrolyte were collected, dried and analyzed by XRD (orange line) revealing the presence of Simonkolleite, ZnO and Zn.

Until now, it could be concluded that Simonkolleite and possibly ZnO are the main components of the passive film when Zn is discharged in the neat 2 M NaCl. But as shown in

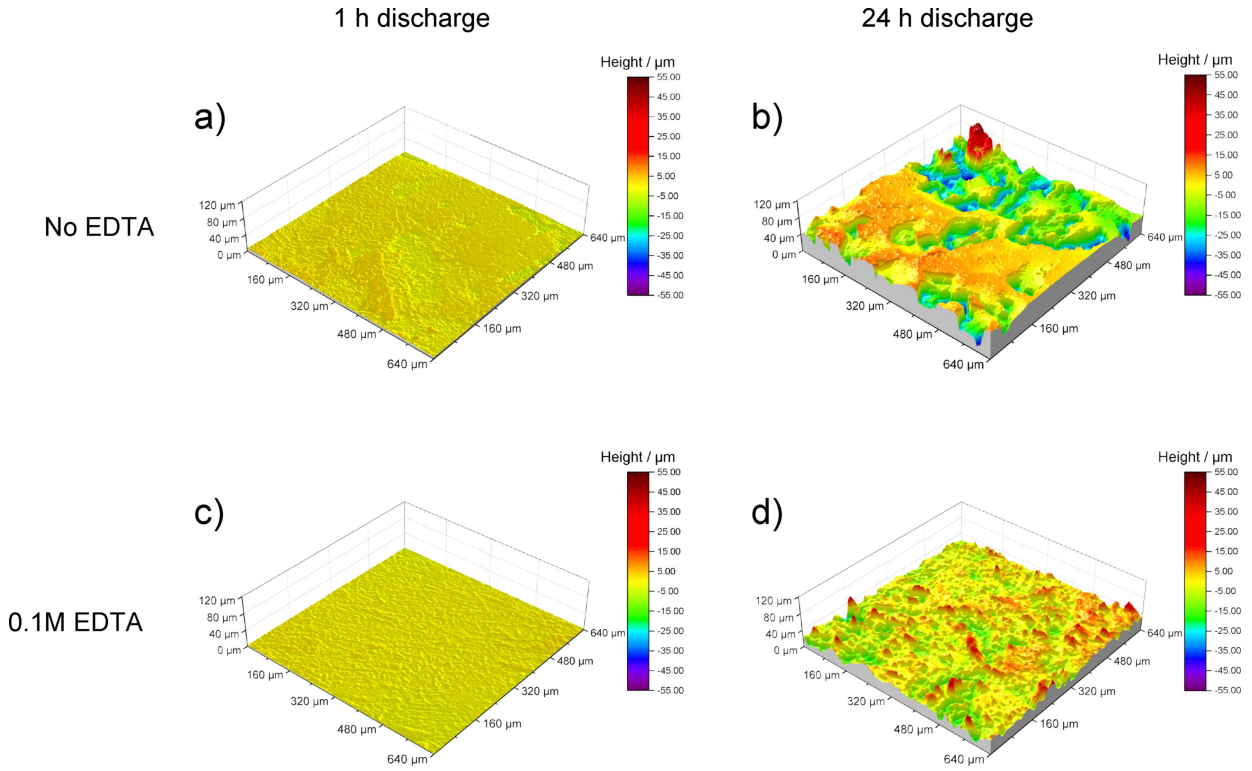

Figure 4. Laser scanning microscopy images of Zn discharged in 2 M NaCl pH 10 in absence (a, b) and presence of EDTA (c, d) after 1 h (a, c) and 24 h (b, d) with 1 mA cm^{-2}. Yellow/orange areas in (b) represent the passive layer formed after 24 h of discharge in neat 2 M NaCl pH 10.

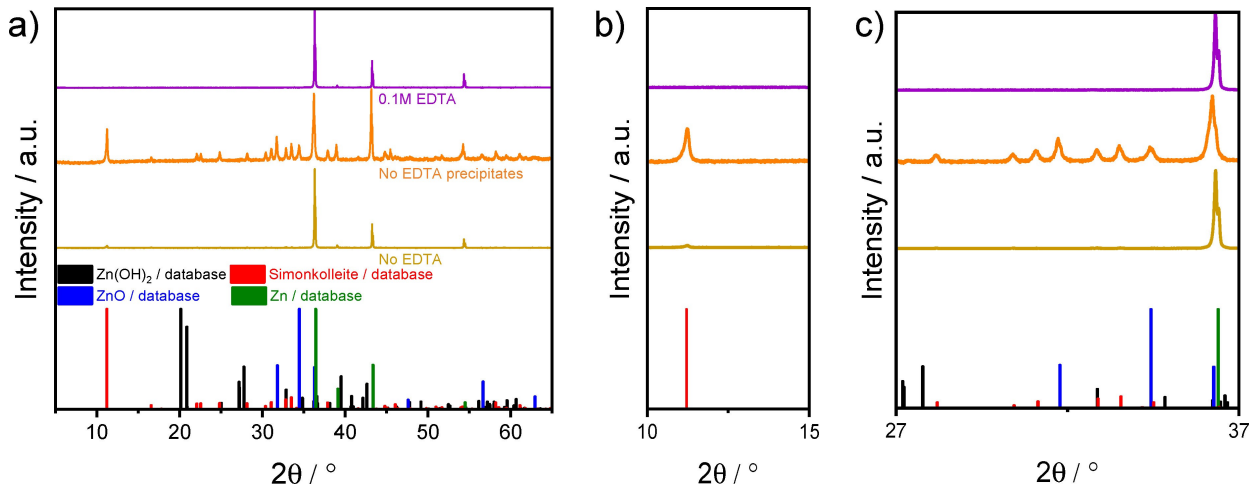

Figure 5. a) XRD patterns of Zn discharged in 2 M NaCl at pH 10 with and without EDTA under 1 mA cm^{-2} after 24 h, b) enlarged region of the peaks between 10 and 15° and c) enlarged region of the peaks between 27 and 37°.

Equations (5) and (7), the production of Simonkolleite and ZnO requires $Zn(OH)_2$ as an intermediate step. Thus, the passive layer on the Zn discharged in neat electrolyte should also show the presence of $Zn(OH)_2$, but the amount might be too small to be identified by XRD or it may be amorphous. Similarly, if a thin $Zn(OH)_2$ passive layer is also present on the Zn after discharge in presence of 0.1 M EDTA, it might not be possible to be detected by XRD.

In order to gain further insights into the surface products of the Zn electrodes, scanning electron microscopy (SEM) imaging coupled to energy dispersive spectroscopy element analysis (EDX) was carried out. Figure 6 shows the SEM images and EDX

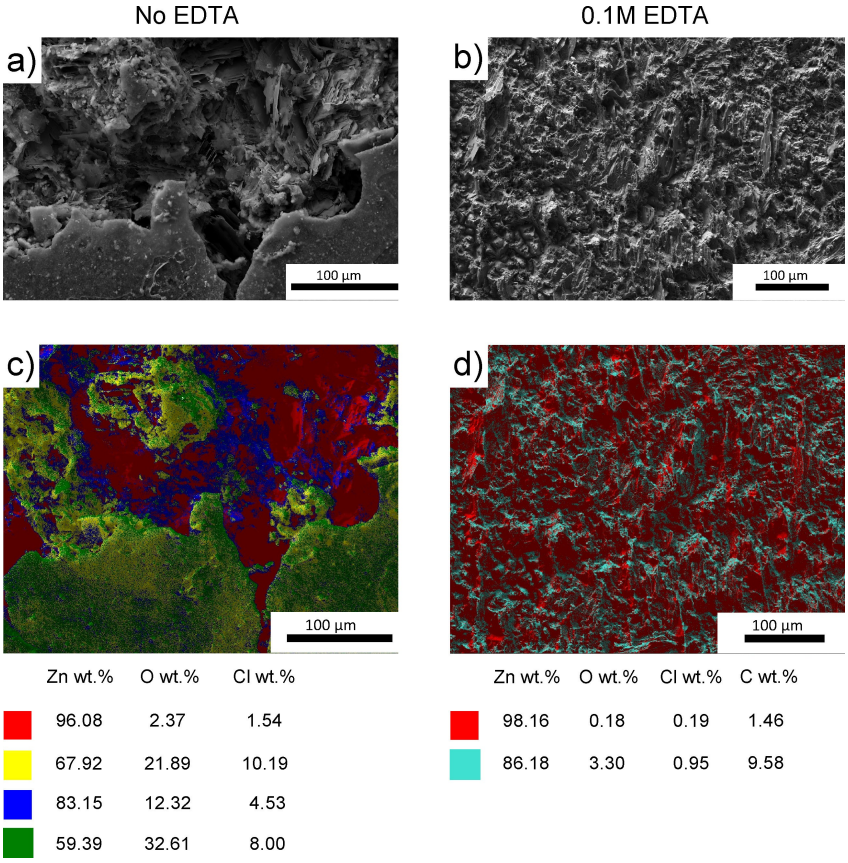

Figure 6. SEM images (a, b) and EDX maps (c, d) of Zn discharged for 24 h at 1 mA cm^{-2} in 2 M NaCl pH 10 without (a, c) and with 0.1 M EDTA (b, d). The weight distribution of the EDX maps is provided below the figure.

maps of Zn after 24 h of discharge at 1 mA cm^{-2} in 2 M NaCl without and with 0.1 M EDTA. The Zn surface in Figure 6a (no EDTA) shows the microstructure of the region where the passive film extends over the metallic Zn. The EDX map in Figure 6c depicts a better contrast between the film and the metallic Zn. The SEM image in Figure 6b (0.1 M EDTA) illustrates a surface without any apparent layer on top of the Zn surface, while the EDX map in Figure 6d shows two regions containing mostly Zn. The elemental distribution is provided in Table 2. The individual elemental maps of Figures 6c and d are provided in Figure S3. Also, the SEM images and elemental maps for 1 h discharged surfaces can be found in the Supporting Information (Figure S1, S2, and Table S2).

The sample discharged in neat 2 M NaCl under 1 mA cm^{-2} in Figure 6c shows four different regions. The red region corresponds to metallic Zn. The yellow region has an elemental composition that is close to Simonkolleite. The blue and green regions are attributed to ZnO and $Zn(OH)_2$ respectively while neglecting the Cl content. Figure 6d shows two regions on the Zn surface that was discharged in 2 M NaCl containing 0.1 M EDTA. The red region corresponds to pure Zn with probably some EDTA still adsorbed. The cyan region has a composition that is also very close to metallic Zn with additional ~10 wt% C. The difference between the red and the cyan region can be attributed to the possibly different amount of remaining adsorbed EDTA on the Zn surface

Considering the Equations (3) – (7) in addition to the results provided by XRD, SEM and EDX analysis are important to determine the nature of the passive film forming on Zn upon discharge in 2 M NaCl without EDTA. Equation (3) shows that $Zn(OH)_2$ can be formed following the oxidation of Zn to Zn^{2+}. Upon local saturation of $Zn(OH)_2$, ZnO or Simonkolleite can be formed. However, as revealed by the XRD and EDX results, Simonkolleite can be found only after long discharge time (at least 24 h). Thus ZnO could be assumed as a second component of the passive film, besides the $Zn(OH)_2$. However, it is noteworthy to mention that the surface of the Zn electrodes could possibly be changing while cleaning and transferring into other characterization tools after the electrochemical investigations. Hence, for example, ZnO might mainly be detected instead of $Zn(OH)_2$ although the latter may be the main product during the electrochemical studies, as previously described by Equation (5). Once the $ZnO/Zn(OH)_2$ passive film is formed over the neat Zn, the reaction continues as dictated by Equation (7) and Simonkolleite is formed. Moreover, this passive film grows until forming scales, which breaks upon the mechanical stress of the volume increase (see Table S1) and some pieces might precipitate. Support for this idea can be observed in the SEM images (surface films in Figure 6a and Figure S2), besides the flakes found in the sediments after 24 h of discharge. Additionally, the XRD results after 24 h of discharge (Figure 5) show a high presence of Simonkolleite in the sediments collected, while the intensity peaks of Simonkolleite on the Zn electrode after discharge were not significant. However, some amount of Simonkolleite was detected by EDX (Figure 6c and Table 2). Thus it could be concluded that the thin passive film on Zn upon discharge in 2 M NaCl without EDTA consists of a combination of $ZnO/Zn(OH)_2$ and Simonkolleite.

Conversely, the addition of EDTA to the 2 M NaCl interferes with the formation of a passive film by complexing the Zn directly after its oxidation [Eq. (2)], as evidenced by the SEM, EDX and LSM results. Furthermore, the electrolyte has no precipitates and remains clear after discharging the Zn in presence of EDTA, implying that the Zn-EDTA complex remains solvated.

Accordingly, the following mechanism can be proposed for the OCP and discharge experiments of Zn in 2 M NaCl pH 10 with 0.1 M EDTA. The EDTA is directly adsorbed on the Zn surface upon immersion of the electrode by possibly interacting with the metallic surface.[46,47] After the spontaneous (OCP conditions) reaction or anodic oxidation (discharge conditions) of Zn to Zn^{2+}, the adsorbed EDTA chelates and captures the Zn^{2+} limiting the formation of ZnO, $Zn(OH)_2$ or Simonkolleite as schematically shown in Figure 7. The Zinc-EDTA complex remains as an aqueous specie, thus avoiding the formation of a passive film. The inhibition of passive film formation leaves the next layer of metallic Zn available to continue with the reaction and no potential drop is expected with enough EDTA to continue the chelation process. Such limitation is therefore of interest in a full-cell experiments over extended periods of discharge.

Table 2. Theoretical element weight distribution of Zn corrosion products and EDX elemental analysis of Zn after 24 h discharge at 1 mA cm^{-2} in 2 M NaCl pH 10 with and without 0.1 M EDTA.

		Zn [wt%]	O [wt%]	Cl [wt%]	C [wt%]
Theoretical	ZnO	80.34	19.66		
	$Zn(OH)_2$[a]	67.14	32.86		
	$Zn_5(OH)_8Cl_2 \cdot H_2O$[a] (Simonkolleite)	60.33	26.58	13.09	
Zn in 2 M NaCl	Zn/O phase (red)	96.08	2.37	1.54	
	Zn/Cl/O phase (yellow)	67.92	21.89	10.19	
	Zn/O phase (blue)	83.15	12.32	4.53	
	Zn/O phase (green)	59.39	32.61	8.00	
Zn in 2 M NaCl with 0.1 M EDTA	Zn phase (red)	98.16	0.18	0.19	1.46
	Zn/O/Cl/C phase (cyan)	86.18	3.30	0.95	9.58

[a] The elemental weight distribution was calculated omitting the H, since EDAX cannot detect H.

2.4. Full-Cell Galvanostatic Discharge Experiments

Figure 8 shows the full-cell galvanostatic discharge profiles of Zn in 2 M NaCl pH 10 electrolytes under 0.25, 0.5 and 1 mA cm^{-2} in absence (black curves) and presence of 0.1 M EDTA (red curve). The open circuit voltage (OCV) of Zn in the neat 2 M NaCl is around 1.1 V, while the discharge voltages are similar among all the applied currents at around 0.9 V during the first hours. However, the Zn discharged in neat electrolyte under 0.25 mA cm^{-2} shows a fluctuating voltage after 291 h and reached a total of 931 h, whereas it could be discharged

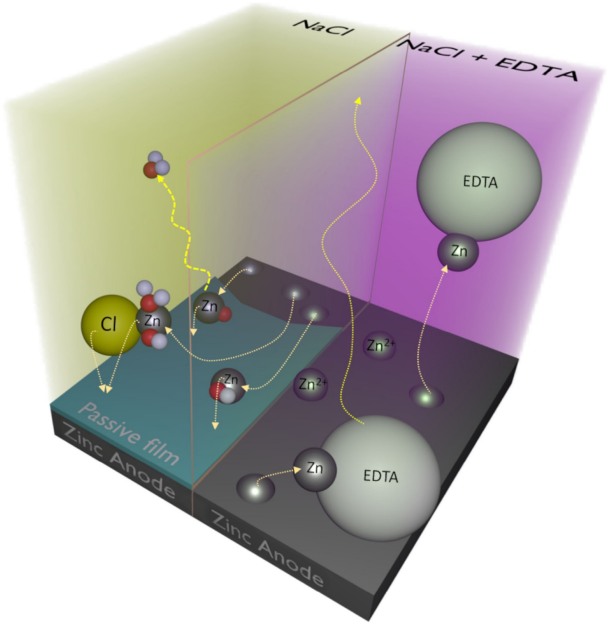

Figure 7. Schematic representation of the complexation process and possible differences on Zn surfaces that are in contact with the neat NaCl and NaCl + EDTA solutions. For simplicity, the ions and the molecules are shown in spherical shapes.

under 0.5 and 1 mA cm^{-2} for a total of 255 and 110 h, respectively.

The OCV of Zn in 2 M NaCl with 0.1 M EDTA is at around 1.4 V, while the discharge voltage under the applied currents is similar at around 1.1 to 1.15 V. The overall discharge voltage enhancement provided by the addition of EDTA to the electrolyte is around 270 to 320 mV higher in comparison to the neat electrolyte. Nevertheless, the discharge voltage of Zn in presence of EDTA noticeably decreases after 600 h under 0.25 mA cm^{-2}, after 270 h under 0.5 mA cm^{-2} and after 101 h under 1 mA cm^{-2}. The resulting values after the voltage drop are then similar to the respective cell voltages without EDTA. It is noteworthy to mention that there were strong fluctuations on the cell voltages most likely due to discharge via pitting mechanism after the effect of EDTA was lost. The cells containing EDTA could be operated in total up to 931 h under 0.25 mA cm^{-2}, 330 h under 0.5 mA cm^{-2} and 146 h under 1 mA cm^{-2}.

In order to determine the limiting factor on the enhanced discharge voltage, further experiments under 1 mA cm^{-2} with a 40 mL electrolyte reservoir (vs. 20 mL from Figure 8) were performed (see Figure S4a), showing a significant increase of the discharge time with similar discharge voltages to those presented in Figure 8c. Thus, the total amount of EDTA available in the electrolyte for the discharge plays an important role for extending the improved discharge energies of Zn–air batteries.

In comparison to similar near-neutral battery systems under the same discharge current densities,[14,16,26] the addition of EDTA to the electrolyte shows noteworthy higher discharge voltages (1 V vs 1.15 V, respectively), which are also fairly comparable to the voltages observed in alkaline systems (1.25 V_{KOH} vs 1.15 V_{NaCl} at 1 mA cm^{-2}).[14,58] Besides the cell voltage enhancement, all the full-cell discharge experiments performed with the electrolyte containing EDTA exhibited no deposits on the electrode surfaces, while the electrolyte was also almost free of precipitates. Conversely, the cell discharged with neat 2 M NaCl electrolyte showed a thick white layer covering the air-electrode, which probably led to clogging and stopped the discharge. Similarly, large amounts of precipitates could be found in the used 2 M NaCl without EDTA and the Zn anode was also covered with a thick white layer.

As discussed in the half-cell stripping section, a passive film forming upon contact of Zn with the neat 2 M NaCl could also explain the relatively low OCV and discharge voltage of the full-cell, besides the poor pH stability of NaCl and formation of insoluble reaction products (such as Simonkolleite). In contrast, the enhanced voltage observed for the cells containing EDTA could be attributed to the absence of film formation resulting from the chelating properties of EDTA. Therefore, the surface of the discharged samples in the full-cell setup was further analyzed by XRD in order to detect possible reaction products which could explain the observed discharge voltages.

Figure 9 presents the XRD patterns of the samples after the long-run full-cell discharge experiment from Figure 8. The XRD results show the presence of Simonkolleite on the Zn electrodes discharged under 1 mA cm^{-2} in neat 2 M NaCl (purple line), while the XRD patterns after discharged in 2 M NaCl with 0.1 M

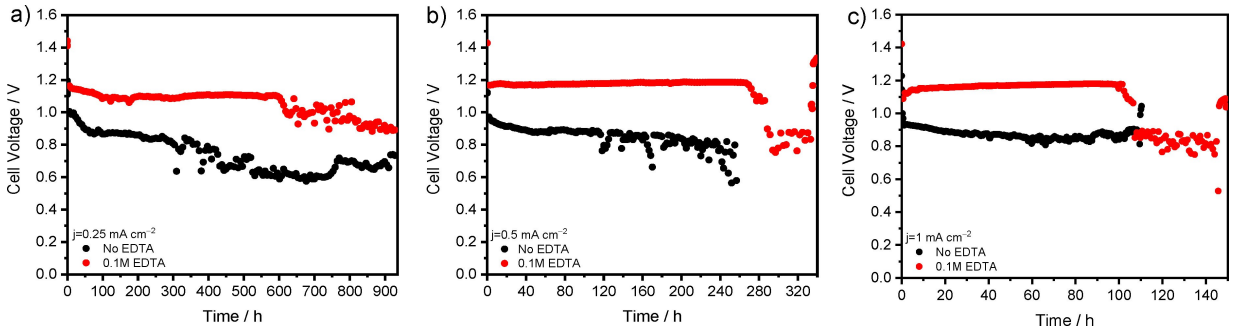

Figure 8. Full-cell galvanostatic discharge profiles of Zn in 2 M NaCl at pH 10 in absence (black curves) and presence (red curves) of 0.1 M EDTA under a) 0.25 mA cm^{-2}, b) 0.5 mA cm^{-2}, c) 1 mA cm^{-2}.

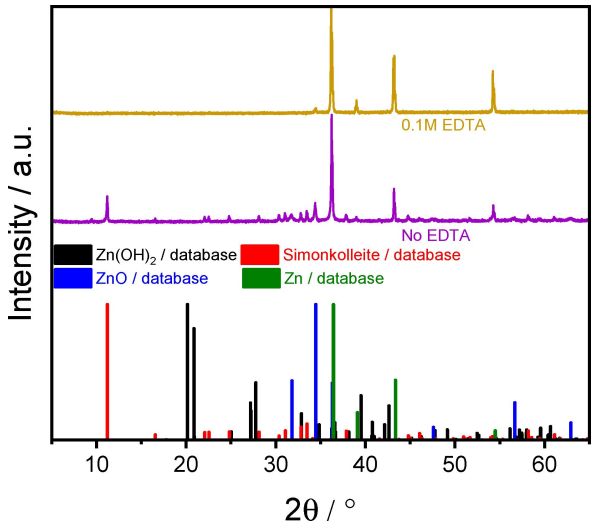

Figure 9. XRD pattern of Zn samples discharged in full-cells under 1 mA cm^{-2} in 2 M NaCl pH 10 in absence (purple) and presence (yellow) of 0.1 M EDTA.

EDTA electrolyte illustrate almost exclusively the peaks for metallic Zn (yellow line). Furthermore, the XRD analysis of Zn discharged with a larger reservoir volume show Simonkolleite in absence of EDTA and only the Zn peaks in presence of EDTA (see Figure S4b). Based on the present results, it could be argued that the Simonkolleite is the main component of the passive film of Zn in presence of neat 2 M NaCl, but the presence of ZnO and $Zn(OH)_2$ underneath the Simonkolleite layer cannot be conclusively discarded as shown by the previous EDX analysis. In the case of the Zn discharged with EDTA, there are no indications for a film formation from the XRD results.

Table 3 presents a summary of the practical capacity, practical specific energy and mass utilization efficiency calculated after the discharge of Zn in 2 M NaCl in absence and presence of 0.1 M EDTA under several current densities. The calculation of the values was based on the total mass loss of the discharged Zn anodes. The practical capacity of Zn discharged in neat 2 M NaCl is in average 744 mAh g_{Zn}^{-1}, while the average practical specific energy is 573 Wh kg_{Zn}^{-1}. The overall utilization efficiency is around 90 %. Contrariwise, the cells discharged in presence of 0.1 M EDTA showed an increase in the practical capacity with an average of 779 mAh g_{Zn}^{-1}. The practical specific energy shows a significant increase with an average of 833 Wh kg_{Zn}^{-1}, which is around 45 % higher than for the cells discharged in neat 2 M NaCl. The overall average mass utilization efficiency for the cells discharged in presence of 0.1 M EDTA is 95 %, which is slightly higher than the cells discharged in absence of EDTA.

The enhanced practical specific energy of the cells discharged in presence of EDTA is explained by the higher discharge voltage in comparison to the cells discharged in absence of EDTA. The data in Table 3 shows that the most efficient cells are those discharged in 2 M NaCl with 0.1 M EDTA under 0.25 mA cm^{-2}, where the enhanced voltage lasts almost until the end of the experiment. The latter suggests that even higher practical specific energies and mass utilization efficiencies could be achieved with non-interrupted enhanced voltages, specifically if enough EDTA is provided to achieve longer runs. All in all, the discharge of Zn in a full-cell is possible with 2 M NaCl in absence and in presence of 0.1 M EDTA, while the latter depicts better performances.

2.5. Full-Cell Galvanostatic Cycling

The possible beneficial effects of EDTA as additive for NaCl electrolytes should be further extended to not only primary Zn–air batteries, but also for secondary batteries, as suggested by earlier studies in alkaline media. Thus, the evaluation of the effects of EDTA on Zn upon charging in NaCl solutions is relevant to establish an initial framework since no previous works exist to the knowledge of the authors.

Figure 10 shows the galvanostatic full-cell cycling profiles (at low depth of discharge) under 0.5 mA cm^{-2} current densities for 4 h per step (charge and discharge). The cycling of Zn in neat 2 M NaCl (black curve) shows an average discharge voltage at around 0.86 V and charging voltages at around 1.59 V, which results in a 0.73 V voltage difference. The cells cycled in presence of EDTA (red curve) showed an average discharge voltage around 1.15 V and an average charge voltage at around 1.62 V although at the initial cycles, the cell with the EDTA additive exhibited slightly higher charging voltages in comparison to the cell with the neat electrolyte. The origin of such higher charging voltage, whether it is from the air cathode or from the initial Zn-EDTA complexes is not clear and requires further investigations. The average discharge voltage in presence of EDTA is 290 mV higher than without EDTA. The smaller discharge/charge voltage difference in presence of EDTA

Table 3. Practical capacity, practical specific energy and mass utilization efficiency calculated after the discharge of Zn in 2 M NaCl pH 10 in absence and presence of 0.1 M EDTA under several currents.

Electrolyte	Current density [mA cm^{-2}]	Practical capacity [mAh g_{Zn}^{-1}]	Practical specific energy [Wh kg_{Zn}^{-1}]	Mass utilization efficiency [%]	Discharge time Enhanced [h]	Total [h]
2 M NaCl	0.25	751.1 ± 3.5	535.8 ± 17.4	91.6 ± 0.4	–	931
	0.5	735.1 ± 17.3	574.9 ± 65.5	89.6 ± 2.1	–	255
	1	748.4 ± 18.7	611.0 ± 28.2	91.3 ± 2.3	–	110
2 M NaCl + 0.1 M EDTA	0.25	796.4 ± 5.0	829.5 ± 7.7	97.1 ± 0.6	600	931
	0.5	750.8 ± 35.6	842.3 ± 38.8	91.5 ± 4.3	270	330
	1	791.3 ± 8.6	829.4 ± 23.4	96.5 ± 1.1	101	146

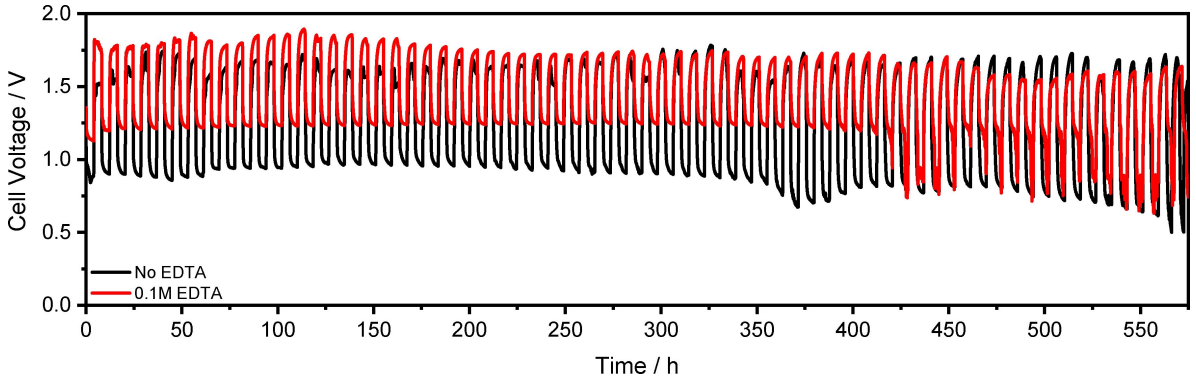

Figure 10. Full-cell galvanostatic cycling of Zn under 0.5 mA cm^{-2} for 4 h per step in 2 M NaCl pH 10 in absence (black curve) and presence (red curve) of 0.1 M EDTA.

indicates less overpotentials, which is beneficial for battery applications.

Considering the cycling stability, the discharge performance of Zn–air cell with neat 2 M NaCl starts to decay from the 68th cycle after 550 h, eventually leading to termination of the cell operation due to reaching the 0.5 V cut-off voltage rapidly. Similar cycling life was also achieved by the full-cells with 0.1 M EDTA additive while displaying enhanced performance for at least 51 cycles (416 h) with discharge voltages at around 1.25 V. However, the discharge voltage starts to decrease from the 52nd cycle (after 420 h) to around 0.95 V, which is similar to the cells without EDTA. Nevertheless, the discharge voltage of the subsequent cycles partially recovers to 1.2 V for a limited time, and eventually the positive influence of the EDTA additive was almost completely lost for the remaining cycles.

All in all, the full-cell experiments demonstrate the feasibility of cycling of Zn in 2 M NaCl pH 10 with and without 0.1 M EDTA additive. Moreover, the cycling of Zn in the electrolyte containing 0.1 M EDTA shows a better performance in terms of the higher discharge voltage, higher power output and discharge energies. However, further investigations are needed in order to achieve better regeneration of active EDTA, which would result in longer full-cell cycling with enhanced discharge and lower charging voltages. In comparison to other Zn–air batteries with near-neutral electrolytes which are mostly based on NH_4Cl electrolytes[14,26,28] for their high buffering capabilities, this study also provides a possible alternative electrolyte as NaCl-based solutions with additives that prevent passive film formation and also help to stabilize the pH while providing higher discharge voltages. The ability of EDTA to diminish or hinder the formation of passive films could be further extended to other anode materials which suffer from similar constrains in near-neutral electrolytes, while the only limitation is the ability of the EDTA to complex such materials.

3. Conclusions

The influence of ethylenediaminetetraacetic acid (EDTA) electrolyte additive on the electrochemistry of Zn electrodes was investigated in half- and full-cells with near-neutral electrolytes. The OCP experiments showed that the Zn is not completely active in presence of neat 2 M NaCl at pH 10, however, the EDTA additive enhanced the potentials by almost 200 mV. Further evidence of the quasi-passivated state of the Zn in neat 2 M NaCl is found from the galvanostatic discharge, where the discharge potentials under different current densities were similar due to pitting. Conversely, the galvanostatic discharge of Zn in presence of 0.1 M EDTA shows a general enhancement of around 200 mV on the discharge potential under several currents implying a more active surface of the Zn without any pitting. The LSM, SEM and EDX measurements of Zn discharged in neat 2 M NaCl revealed the existence of a passive film composed by Simonkolleite, $Zn(OH)_2$ and/or ZnO, while such a passive film was not present on the Zn surfaces after discharging in the electrolyte containing 0.1 M EDTA.

The oxidation of Zn in presence of neat 2 M NaCl seems to mainly promote the production of insoluble species, which may eventually form a passive film and precipitates in the electrolyte. Contrariwise, the overall enhancement on the cell potentials in presence of EDTA is explained by the chelation of Zn^{2+} ions by the EDTA before formation of hydroxide or oxide species. The complexation process can occur upon adsorption of EDTA on the Zn surface. Consequently, the EDTA prevents the formation of insoluble species such as Simonkolleite, ZnO, or $Zn(OH)_2$ while the produced Zn-EDTA complex remains solvated. Thus, the metallic Zn surface remains active and available for further reaction.

The performance of Zn–air full-cells were investigated by galvanostatic discharge under several current densities. The discharge experiments with neat electrolyte lasted up to 930 h while providing discharge voltages below 1 V. The addition of 0.1 M EDTA to the electrolyte increases the cell discharge voltage to a maximum of 1.2 V. Accordingly, the practical specific energies of Zn are significantly enhanced up to 833 Wh kg_{Zn}^{-1} in presence of EDTA. In addition to the galvanostatic discharge, the Zn–air cells could also be cycled up to 70 cycles with 0.5 mA cm^{-2} while delivering average discharge voltages of 0.86 V in neat electrolyte and 1.15 V in presence of EDTA additive. In both galvanostatic discharge and cycling experiments, the positive effect of EDTA additive on the enhanced discharge voltages lasted for several hundred hours

and is limited only by the available amount of EDTA. Further investigations should focus on the chelation mechanisms of EDTA as well as the recovery of the Zn ions from the complexes upon charging.

Experimental Section

Material preparation and chemicals

Zinc rod (4 N) was acquired from Alfa Aesar. The electrodes were prepared by cutting sections of the Zn rod into 0.125 mm thickness discs. For the half-cell experiments, the Zn discs were embedded in cold mount epoxy (EpoFix, Struers) and the surfaces of the electrodes were prepared by grinding with 800 SiC sandpaper. The exposed area of the electrodes for half-cell and full-cell experiments were 1.32 cm^2 and 0.44 cm^2, respectively.

The 2 M NaCl-based electrolyte solutions were prepared from NaCl crystals ($\geq$99.5 %, Merck-Millipore) and Ethylenediaminetetraacetic acid (EDTA) (99.3 %, VWR Chemicals). Deionized water was obtained from a PURELAB Elga water purification system (conductivity $<0.1\ \mu S\,cm^{-1}$). The electrolyte solutions were prepared by dissolving the NaCl and EDTA in deionized water, and then the pH of all solutions was initially adjusted to pH 10 with NaOH solutions by the help of a dual pH/conductivity meter (Duo S213, Mettler Toledo).

Electrochemical half-cell setup

The half-cell consisted of a three-electrode setup with Zn as working, Pt mesh as counter, and silver/silver chloride (Ag/AgCl in 3 M NaCl) as reference electrodes. The volume of the cell was 20 mL. The potentiodynamic polarization tests were undertaken in the range from $-1.6\ V_{Ag/AgCl}$ to $-0.6\ V_{Ag/AgCl}$ starting from cathodic potentials. Half-cell stripping (or galvanostatic discharge) was performed under 0.1, 0.25, 0.5 and 1 $mA\,cm^{-2}$ current densities with a cut-off potential of $-0.5\ V_{Ag/AgCl}$.

Electrochemical full-cell setup

The full-cell setup consisted of freshly ground Zn discs as anode, porous carbon-based commercial air electrodes (E4 type, Electric Fuel Ltd), and 2 M NaCl with pH 10 with and without addition of EDTA (0.1 M). The full-cell is made of three poly(methyl methacrylate)) (PMMA) discs with an inner volume of 0.6 mL. The details of the cell setup can be found in a previous study.[59] The symmetrical exposed area of the anode and air cathode to the electrolyte was 0.44 cm^2. The cell was connected to a pump (Reglo Analog MS-4/112, Ismatec) and to a reservoir with capillary tubes ($\varnothing_{in} = 0.75$ mm. PEEK, BOLA). The electrolyte was circulating in bottom-top direction. Both ends of full-cell were connected to the same reservoir which contained 20 mL of the electrolyte. Following the discharge experiments, the weight loss of the Zn electrodes were calculated after cleaning with saturated Glycine solution according to DIN EN ISO 8407.[60]

A continuous recirculation of the electrolyte from a reservoir was performed for the full-cell discharge experiments. The electrolyte of the full-cell cycling experiments was circulated by pumping every 25 min for 5 min with a flow rate of 0.1 $mL\,min^{-1}$ for each cell in order to provide enough dissolved Zn. The intermittent operation of the pump was controlled by a TTL pulse via the analogue connection of the Biologic VMP3 potentiostat.

All the experiments were conducted in a climate chamber (Binder KMF115) to keep constant conditions of 25 °C and 50 % r.h. and electrochemical experiments were controlled with a Biologic VMP3 potentiostat.

Sample analysis and microscopy

Characterization of the microstructures of the Zn anodes after discharge was done by confocal laser scanning microscopy (OLS4100, Olympus Corp., Japan) and scanning electron microscopy (Quanta 650, FEI, USA) using the Everhart-Thornley Detector (ETD). The elemental analysis was performed by energy-dispersive X-ray spectroscopy (EDX) (Octane Super Detector, EDAX, USA) and the corresponding phase maps were obtained by using TEAM EDAX software. The SEM measurements were performed with 20 kV of applied acceleration voltages. Crystallographic characterization of the Zn anode surfaces was performed by X-ray diffraction (XRD) (Cu-source Empyrean, Malvern Panalytical, Germany).

Acknowledgements

This research was funded by the German Federal Ministry of Education and Research (BMBF) within the project 'MeLuBatt' "Frischer Wind für Metall-Luftsauerstoff Batterien: Was man von Li-Ionen Batterien lernen kann" (project no. 03XP0110F). S.B. acknowledges Electroscopy (Grant No. 892916) from the Marie Skłodowska-Curie action. Open access funding enabled and organized by Projekt DEAL.

Conflict of Interest

The authors declare no conflict of interest.

Keywords: additive · EDTA · metal–air battery · neutral aqueous electrolyte · zinc–air

[1] A. R. Mainar, E. Iruin, L. C. Colmenares, A. Kvasha, I. de Meatza, M. Bengoechea, O. Leonet, I. Boyano, Z. Zhang, J. A. Blazquez, *J. Energy Storage* **2018**, *15*, 304–328.
[2] J. Ryu, M. Park, J. Cho, *Adv. Mater.* **2019**, *31*, 1804784.
[3] H. Weinrich, Y. E. Durmus, H. Tempel, H. Kungl, R.-A. Eichel, *Materials (Basel).* **2019**, *12*, 2134.
[4] W.-J. Kwak, Rosy, D. Sharon, C. Xia, H. Kim, L. R. Johnson, P. G. Bruce, L. F. Nazar, Y.-K. Sun, A. A. Frimer, M. Noked, S. A. Freunberger, D. Aurbach, *Chem. Rev.* **2020**, *120*, 6626–6683.
[5] Q. Liu, Z. Pan, E. Wang, L. An, G. Sun, *Energy Storage Mater.* **2020**, *27*, 478–505.
[6] J. Fu, Z. P. Cano, M. G. Park, A. Yu, M. Fowler, Z. Chen, *Adv. Mater.* **2017**, *29*, 1604685.
[7] N. Borchers, S. Clark, B. Horstmann, K. Jayasayee, M. Juel, P. Stevens, *J. Power Sources* **2021**, *484*, 229309.
[8] Y. Li, H. Dai, *Chem. Soc. Rev.* **2014**, *43*, 5257–5275.
[9] Y. Li, J. Lu, *ACS Energy Lett.* **2017**, *2*, 1370–1377.
[10] Z. P. Cano, D. Banham, S. Ye, A. Hintennach, J. Lu, M. Fowler, Z. Chen, *Nat. Energy* **2018**, *3*, 279–289.
[11] D. Stock, S. Dongmo, J. Janek, D. Schröder, *ACS Energy Lett.* **2019**, *4*, 1287–1300.
[12] P. Pei, K. Wang, Z. Ma, *Appl. Energy* **2014**, *128*, 315–324.
[13] X. Chen, Z. Zhou, H. E. Karahan, Q. Shao, L. Wei, Y. Chen, *Small* **2018**, *14*, 1801929.
[14] A. Sumboja, X. Ge, G. Zheng, F. W. T. Goh, T. S. A. Hor, Y. Zong, Z. Liu, *J. Power Sources* **2016**, *332*, 330–336.

[15] L. Li, A. Manthiram, *Adv. Energy Mater.* **2016**, *6*, 1502054.
[16] S. Clark, A. R. Mainar, E. Iruin, L. C. Colmenares, J. A. Blázquez, J. R. Tolchard, Z. Jusys, B. Horstmann, *Adv. Energy Mater.* **2020**, *10*, 1903470.
[17] W. Sun, F. Wang, B. Zhang, M. Zhang, V. Küpers, X. Ji, C. Theile, P. Bieker, K. Xu, C. Wang, M. Winter, *Science.* **2021**, *371*, 46–51.
[18] T. N. T. Tran, M. P. Clark, H. Chung, D. G. Ivey, *Batteries and Supercaps* **2020**, *3*, 409–416.
[19] T. N. T. Tran, D. Aasen, D. Zhalmuratova, M. Labbe, H. Chung, D. G. Ivey, *Batteries and Supercaps* **2020**, *3*, 917–927.
[20] S. Chen, S. Chen, J. Zhang, *Batteries & Supercaps* **2019**, *2*, 373–379; Supercaps **2019**, 2, 373–379.
[21] S. S. Shinde, J. Y. Jung, N. K. Wagh, C. H. Lee, D.-H. Kim, S.-H. Kim, S. U. Lee, J.-H. Lee, *Nat. Energy* **2021**.
[22] X. G. Zhang, *Corrosion and Electrochemistry of Zinc*, Springer US, Boston, MA, **1996**, pp. 220–227, 373–377.
[23] D. Linden, T. B. Reddy, *Handbook of Batteries*, McGraw-Hill, New York, **2002**.
[24] J. Jindra, J. Mrha, M. Musilova, *J. Appl. Electrochem.* **1973**, *3*, 297–301.
[25] S. Amendola, M. Binder, P. J. Black, S. Sharp-Goldman, L. Johnson, M. Kunz, M. Oster, T. Chciuk, R. Johnson, *Electrically Rechargeable, Metal-Air Battery Systems and Methods*, **2012**, US2012/0021303 A1.
[26] F. W. T. Goh, Z. Liu, T. S. A. Hor, J. Zhang, X. Ge, Y. Zong, A. Yu, W. Khoo, *J. Electrochem. Soc.* **2014**, *161*, A2080–A2086.
[27] S. Clark, A. Latz, B. Horstmann, *ChemSusChem* **2017**, *10*, 4735–4747.
[28] S. Clark, A. R. Mainar, E. Iruin, L. C. Colmenares, J. A. Blázquez, J. R. Tolchard, A. Latz, B. Horstmann, *J. Mater. Chem. A* **2019**, *7*, 11387–11399.
[29] Y. E. Durmus, S. S. Montiel Guerrero, H. Tempel, F. Hausen, H. Kungl, R.-A. Eichel, *Front. Chem.* **2019**, *7*, 800.
[30] A. R. Mainar, L. C. Colmenares, J. A. Blázquez, I. Urdampilleta, *Int. J. Energy Res.* **2018**, *42*, 903–918.
[31] G. Juhel, B. Beden, C. Lamy, J. M. Leger, R. Vignaud, *Electrochim. Acta* **1990**, *35*, 479–481.
[32] C. W. Lee, K. Sathiyanarayanan, S. W. Eom, H. S. Kim, M. S. Yun, *J. Power Sources* **2006**, *159*, 1474–1477.
[33] J. C. Ballesteros, E. Chaînet, P. Ozil, G. Trejo, Y. Meas, *Electrochim. Acta* **2011**, *56*, 5443–5451.
[34] V. K. Nartey, L. Binder, K. Kordesch, *J. Power Sources* **1994**, *52*, 217–222.
[35] Y. Ein-Eli, M. Auinat, D. Starosvetsky, *J. Power Sources* **2003**, *114*, 330–337.
[36] Z. Yazicigil, Y. Oztekin, A. Kadir Ince, *Desalin. Water Treat.* **2009**, *11*, 167–172.
[37] M.-C. Huang, S.-H. Huang, S.-C. Chiu, K.-L. Hsueh, W.-S. Chang, C.-C. Yang, C.-C. Wu, J.-C. Lin, *J. Chin. Chem. Soc.* **2018**, *65*, 1239–1244.
[38] S. Fashu, C. Gu, J. Zhang, M. Huang, X. Wang, J. Tu, *Trans. Nonferrous Met. Soc. China* **2015**, *25*, 2054–2064.
[39] N. M. Pereira, S. Salomé, C. M. Pereira, A. Fernando Silva, *J. Appl. Electrochem.* **2012**, *42*, 561–571.
[40] S. Anwar, F. Khan, Y. Zhang, *Mater. Today: Proc.* **2019**, *28*, 532–537.
[41] D. C. Harris, *Quantitative Chemical Analysis*, W. H. Freeman And Company, New York, **2007**, pp. 147. 228–249.
[42] N. N. Greenwood, A. Earnshaw, *Chemistry of the Elements*, Elsevier, Oxford, **1997**, pp. 906–911.
[43] M. E. McMahon, R. J. Santucci, J. R. Scully, *RSC Adv.* **2019**, *9*, 19905–19916.
[44] M. Pourbaix, *Atlas of Electrochemical Equilibria in Aqueous Solutions*, National Association Of Corrosion Engineers, Houston, TX, **1974**, pp. 406–413
[45] B. Beverskog, I. Puigdomenech, *Corros. Sci.* **1997**, *39*, 107–114.
[46] J. Ryczkowski, *Appl. Surf. Sci.* **2005**, *252*, 813–822.
[47] G. A. Parks, *Chem. Rev.* **1965**, *65*, 177–198.
[48] J. A. Rumball, G. D. Richmond, *Int. J. Miner. Process.* **1996**, *48*, 1–20.
[49] H. Tamura, N. Ito, M. Kitano, S. Takasaki, *Corros. Sci.* **2001**, *43*, 1675–1691.
[50] M. Kuśmierz, S. Pasieczna-Patkowska, *Ann. UMCS, Chem.* **2014**, *68*, 25–31.
[51] M. Prestat, J. Soares Costa, B. Lescop, S. Rioual, L. Holzer, D. Thierry, *ChemElectroChem* **2018**, *5*, 1203–1211.
[52] L. M. Baugh, *Electrochim. Acta* **1979**, *24*, 657–667.
[53] H. Leidheiser, Y. Momose, R. D. Granata, *Corrosion* **1982**, *38*, 178–179.
[54] K. Bae, J. La, I. Lee, S. Lee, K. Nam, *Met. Mater. Int.* **2017**, *23*, 481–487.
[55] L. Hao, G. Lv, Y. Zhou, K. Zhu, M. Dong, Y. Liu, D. Yu, *Materials (Basel).* **2018**, *11*, 2307.
[56] K. Aramaki, *Corros. Sci.* **2001**, *43*, 1985–2000.
[57] S. Thomas, N. Birbilis, M. S. Venkatraman, I. S. Cole, *Corrosion* **2012**, *68*, 015009–1.
[58] D. Schröder, N. N. Sinai Borker, M. König, U. Krewer, *J. Appl. Electrochem.* **2015**, *45*, 427–437.
[59] Y. E. Durmus, Ö. Aslanbas, S. Kayser, H. Tempel, F. Hausen, L. G. J. de Haart, J. Granwehr, Y. Ein-Eli, R.-A. Eichel, H. Kungl, *Electrochim. Acta* **2017**, *225*, 215–224.
[60] *DIN EN ISO 8407 : 2014-6*, **2014**.

Manuscript received: May 28, 2021
Revised manuscript received: July 6, 2021
Accepted manuscript online: July 19, 2021
Version of record online: August 6, 2021